An experimental methodology to relate local strain to microstructural texture

J. Carroll,[1] W. Abuzaid,[1] J. Lambros,[2,a)] and H. Sehitoglu[1]
[1]*Mechanical Science and Engineering, University of Illinois at Urbana-Champaign, 160 Mechanical Engineering Building, 1206 W. Green St., Urbana, Illinois 61801, USA*
[2]*Aerospace Engineering, University of Illinois at Urbana-Champaign, 306 Talbot Laboratory, 104 S. Wright St., Urbana, Illinois 61801, USA*

(Received 1 June 2010; accepted 7 July 2010; published online 23 August 2010)

This paper introduces an experimental methodology for obtaining high resolution full-field strain measurements in polycrystalline metals. The (sub)grain level resolution of these measurements was indispensable for relating measured strain fields to observed microstructure in the material. Microstructural information was obtained through electron backscatter diffraction and the optical technique of digital image correlation (DIC) was used to acquire full-field deformation measurements. By spatially overlaying both sets of results, the effects of different microstructural features such as orientation, grain boundary character, misorientation between grains, and twin boundaries on material response can be quantitatively studied. To obtain the necessary resolution for such measurements, the images used in DIC had to be captured at high magnifications. This necessity reduces the field of view and constrains the area of interest that can be monitored. To address this issue, results from adjacent measurement areas are combined together to create a data set with high spatial strain resolution over a larger region than can otherwise be observed. The procedure for performing this technique is outlined here, along with benefits, drawbacks, possible modifications, and example applications of the technique to cyclic plasticity and fatigue crack growth. © *2010 American Institute of Physics.* [doi:10.1063/1.3474902]

I. INTRODUCTION

In the simplest characterizations of polycrystalline material behavior, local microstructural effects are neglected as materials are assumed to be homogeneous and isotropic. These assumptions have proven to be sufficient for many circumstances, but it is increasingly evident that in many cases, local microstructural effects cannot be ignored, necessitating an improved understanding of the physics behind material deformation at the grain level. This understanding can be used to develop microstructure-based models, such as so-called crystal plasticity models that have the potential for improved accuracy in the prediction of structural response. Crystal plasticity models were proposed as early as 1928 by Sachs[1] and can be categorized into four types: full constraint models,[1–3] relaxed constraint models,[4] self-consistent models,[5] and finite element models,[6,7] which have become the most popular type with increases in computational efficiency.

While these models do have predictive capabilities, their accurate application is still currently limited to a narrow range of circumstances. Developing more accurate models will require an improved understanding of grain level deformation mechanisms which will, in turn, require grain level experiments that give quantitative measurements on a full-field basis. Conventional experimental techniques do not have this capability and techniques that do are still in their infancy. Several researchers have compared results from crystal plasticity simulations to grain level experimental results.[8–12] Some useful conclusions were obtained, but these studies were hindered by limitations of the experimental techniques used.

The two most common experimental methods that have been used for quantitative, full-field, grain level measurements are grid techniques[8,12,13] and digital image correlation (DIC).[10,11,14–19] Research is being performed to improve the capabilities of both of these techniques. Grid techniques have proven to work well for large amounts of global strain (on the order of unity), but DIC provides more accuracy at lower strain levels, such as those arising from fatigue in common engineering structures.

In addition to the accuracy of strain measurement, the spatial resolution of experimental measurements is important. Obtaining reliable strain measurements that can be compared to microstructure requires a measurement technique with subgrain level spatial resolution. For the DIC technique, which is based on comparison of an image subset before and after deformation,[20] this effectively means that the subset size must be several times smaller than the grain size, thereby allowing many measurement points within each grain. Since subset sizes are typically limited to the range of 31–101 pixels squared, grain size and magnification are the two main parameters that can be varied to attain a large ratio of grain size to subset size. Many researchers have achieved the necessary spatial resolution by using materials with large grain sizes on the millimetric[10,19,21,22] or even centimetric[13]

a)Author to whom correspondence should be addressed. Electronic mail: lambros@illinois.edu.

scale. Such large grain sizes allow DIC images to be taken at relatively low magnifications. There are many benefits of low magnification DIC when compared to experiments at higher magnification, such as larger optical depth of field, easier speckle pattern creation, and easier alignment of strain fields with microstructure. However, since most structural materials have considerably smaller grain sizes (on the order of 100 μm or smaller), it is not clear whether observations of large grain size materials can be directly applied to materials of interest.

The other approach to obtain adequate spatial resolution is to perform experiments at high magnification. Although *in situ* measurements at the grain level are difficult to obtain in conventional load frames, they are necessary for some applications such as dynamic loading. A few researchers have attempted to relate *in situ* strains at the grain level to microstructural measurements. Padilla *et al.*[18] used *in situ* DIC to measure deformation behavior in dynamically loaded Zr specimens. Strain fields were spatially overlaid with microstructural information and the effects of microstructure on deformation behavior were investigated on a statistical basis. However, the relatively low magnification used in the experiments (1.2 μm/pixel) limited the spatial measurement resolution to approximately the size of the grain diameter (48 μm). This resolution, while reasonable for the statistical analysis it was used for, is not sufficient for a pointwise comparison of full-field deformation behavior to microstructure. Bartali *et al.*[14] made higher magnification *in situ* observations of fatigue at the grain level, but were limited by the lack of a good speckle pattern and optical changes to the specimen throughout the test.

Due to difficulties of *in situ* imaging in conventional load frames such as vibrations, optical limitations, and speckle pattern quality, some researchers have built miniature load frames to be used in an optical microscope.[10,16,22] These experiments circumvent the challenges existent in conventional load frames, but they are limited in terms of specimen size and loading capabilities (i.e., it is difficult to perform fatigue or high temperature experiments).

Yet another approach to high magnification experimentation is to perform image correlation with a scanning electron microscope (SEM).[15,23] As with optical microscopy, *in situ* SEM experiments are limited in specimen size and loading type, but the SEM is capable of much higher magnification. Furthermore, since microstructural information is readily obtained in the SEM through electron backscatter diffraction (EBSD), alignment of strain fields with microstructure maps is relatively simple and accurate. However, the use of SEM for strain measurements using DIC (or grid techniques) does have disadvantages. First, since the image capture process takes several seconds, specimen drift during image capture can generate artifacts in measured strain fields. Additionally, image correlation techniques can be affected by SEM image noise such as background noise, carbon contamination buildup that causes darkening in imaged regions, and the visibility of grain boundaries, which degrades speckle pattern quality.

One fundamental limitation of *in situ* techniques is their limitation to a single field of view or a small number of views with separate cameras (e.g., Ref. 24). With adequate spatial resolution for subgrain level DIC measurements, this means *in situ* techniques are effectively limited to observations of a small number of grains. *Ex situ* DIC, in which the specimen is imaged before and after an applied loading, allows multiple imaging regions to be studied at the desired magnification. These regions can be stitched together to provide high resolution DIC data over a larger number of grains. Efstathiou *et al.*[17] demonstrated that this *ex situ* technique can be used to determine the size of a representative volume element for plastic strain accumulation in Ti. The primary drawback of *ex situ* techniques is that they require interruption of the test and removal of the specimen from the load frame for each measurement. Consequently, these techniques are only capable of measuring accumulated strain. Despite their shortcomings, *ex situ* measurements have high spatial resolution which is particularly useful in certain cases, such as measuring fatigue damage accumulation.

To relate to measured strain fields, microstructural information must also be obtained on a full-field basis and aligned with the strain fields. Alignment can be accomplished with features that are visible in both microstructure maps and correlation images. For low magnification experiments, specimen edges are commonly used. At higher magnifications, the use of fiducial markers or grain boundaries is more typical. A straightforward approach to alignment is to etch specimens to visualize grain boundaries in the correlation images.[14,17] This method provides excellent alignment of the two fields, but visible grain boundaries lines can be problematic for digital image correlation since they interfere with the speckle pattern. Furthermore, etching only provides one aspect of microstructural information: grain geometry. Another important aspect of microstructure is grain orientation, which is typically measured using EBSD. Despite its aforementioned disadvantages, using SEM images to measure strain fields is particularly attractive since it allows easy alignment of strain fields with EBSD grain orientation maps. Tschopp *et al.*[15] describes a technique for linking strains to microstructure in a scanning electron microscope with alignment provided by a combination of grain boundaries and fiducial markers.

In this paper, we will present a new technique for measuring strain accumulation over a region covering hundreds of grains with subgrain level resolution and linking those strain fields to microstructural measurements. This method was developed with great consideration to the details and tradeoffs of the techniques discussed earlier. In this method, *ex situ* optical microscopy DIC is used to measure strain fields. Through the techniques of image and data stitching, high resolution fields are obtained over relatively large regions of the specimen. Fiducial markers are then used to align strain fields with microstructural information from EBSD.

The procedure for using this method is described in Sec. II. Section III demonstrates applications of the technique to cyclic plasticity and fatigue crack growth. Some of the challenges of this technique along with the effects of experimental parameters are discussed in Sec. IV. Finally, Sec. V provides a summary and discusses promising applications of the technique.

II. HIGH RESOLUTION *EX SITU* IMAGE CORRELATION PROCEDURE

The *ex situ* DIC procedure consists of six important steps which are meant to ensure that high resolution DIC strain field maps can be precisely combined with comparable resolution microstructural information. These six steps, which will be discussed in detail in the next six subsections (A–F), are: (1) place fiducial markers on the sample to be used for spatial alignment of the various data sets to be collected; (2) gather microstructural information through EBSD measurements; (3) apply a speckle pattern to the specimen and capture reference images in the optical microscope; (4) load the specimen (mechanically, thermally, etc.) such that permanent deformation is achieved and capture images of the deformed specimen; (5) stitch the images and perform DIC; and (6) align the DIC strain field from step (5) with the microstructure obtained with EBSD from step (2) using the fiducial marks placed in step (1).

A. Fiducial markers

One of the major challenges in successfully implementing the *ex situ* DIC technique is to spatially align the data from both sources with subgrain level accuracy. Such alignment requires fiducial markers, features that appear in both sets of data, be placed on the sample under investigation. While any features can be used as markers, certain characteristics are required to guarantee accuracy and precision of the experimental results. Markers should be numerous so that location, scale, and rotation between the two sets of data can be determined. The markers must also be permanent so that they do not change their shape or position on the specimen between the times that each of the data sets is collected. In addition, the fiducial markers should have features small enough to ensure subgrain level alignment. Finally, the markers must not affect measurements or material behavior for the particular loading used.

Vickers marks were chosen as fiducial markers because they satisfy the four criteria discussed above and because they can be placed easily and precisely. To satisfy the first criterion, an asymmetric pattern of five marks (Fig. 1) was used to allow for placement, scale, and rotation alignment of the data sets generated from multiple devices. Second, Vickers marks are permanent, unlike other marking methods that may be altered chemically or physically. Third, the sharp edges of Vickers marks and the ability to separate them by some distance allow for precise alignment. The fourth criterion of markers is not strictly met since indentation marks leave residual stresses in the material in the vicinity of the indentation marks. However, this effect is made relatively insignificant by ensuring that the affected regions are a small portion of the region of interest and by avoiding results very close to marker locations. A typical use of Vickers indentation marks is shown in Fig. 1, where indentation marks are visible in optical images [Fig. 1(b)] and in EBSD results [Fig. 1(c)]. These marks are approximately 25 μm wide each and spread out so that the region bounded by them is 700×800 μm^2. The sharp corners of the marks allow for precision alignment of EBSD with DIC results.

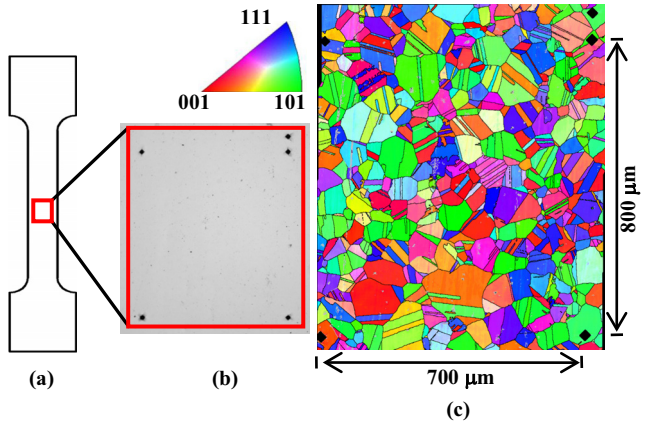

FIG. 1. (Color online) (a) A uniaxial loading specimen showing the region of interest as a red rectangle. (b) Vickers indentation marks on the polished specimen viewed with the optical microscope. (c) Results of the EBSD scan showing grain geometry and orientation in relation to the same Vickers indentation marks as in (b).

B. EBSD measurements

The second step of the *ex situ* procedure is to characterize the microstructure using EBSD.[25] Because standard EBSD sample preparation techniques remove material from the specimen surface due to the subsequent grinding and polishing, Vickers indentation marks are made *after* sample preparation is completed and before placing the specimen into the SEM. Depending on the size of the area of interest, multiple EBSD scans may be needed to span the entire region. It is important that Vickers indentation marks are within the EBSD region for later alignment with DIC measurements. These marks introduce lattice distortions that lead to bad EBSD patterns in the indentation mark locations, thereby making the markers visible in the EBSD image. In this study, EBSD data were collected using a JEOL 7000F SEM with measurement points spaced by 1 μm. Figure 1(c) shows a typical EBSD result consisting of four individual maps stitched together. The five fiducial Vickers marks are clearly visible in the image of Fig. 1(c).

C. Reference images for DIC

Before capturing reference images, a speckle pattern for DIC has to be created. This can be accomplished by depositing 1 μm diameter Si particles onto the specimen surface with compressed air as described in Ref. 26. The reference images have to be acquired with high enough magnification that will guarantee deformation measurements with subgrain level resolution. This DIC resolution requirement, which can be approximated by subset size, is dependent on the magnification level at which images are taken. Higher magnification leads to improved resolution but smaller fields of view. For example, at 50× magnification, a single image covers an area of only 140×104 μm^2. To address this issue, an array of images is taken, with significant overlap among neighboring images, to cover the entire region of interest including the fiducial marks (Fig. 2). As will be shown in this paper, a subset size smaller than the average grain diameter (roughly one fourth) is required for resolving grain level strains in the material. Several magnifications discussed in this paper are

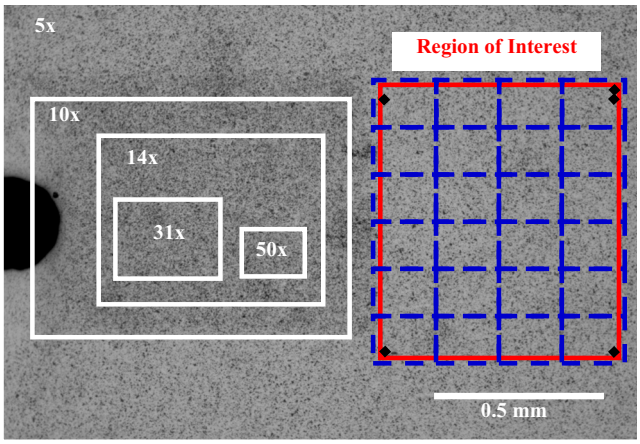

FIG. 2. (Color online) Relative image sizes at several magnifications. The region of interest is imaged at high resolution using an array of high magnification images to cover the region outlined by the indentation marks.

listed in Table I along with their corresponding field of view (compare to Fig. 2), image resolution, subset size, and the ratio of grain area to subset area. Note that these specifications are dependent on a camera's pixel size; hence, the magnification values in Table I are only valid for the camera used in this study. It is emphasized that the required resolution depends on the grain size or other microstructural features present in the material. As those features get smaller in size, images at higher magnifications will be required. Note that because the depth of field at high magnifications is limited and because the distance from the lens to the specimen changes slightly with position, it may be necessary to refocus before capturing each image in the image set. This must be done for both reference and deformed images and is a major obstacle to automation of this process.

D. Deformation

After applying the desired loading to the specimen, e.g., monotonic loading, cyclic loading, thermal loading, etc., the specimen is placed in the optical microscope once again and images of the deformed state are captured at the same locations and magnification as the reference images. The location of each one of those images is determined by visually aligning the observed region with its corresponding reference image. This process of loading and capturing deformed images can be repeated several times as necessary to investigate strain evolution with increased loading. In this paper, we will only show results generated from one loading increment, i.e., one set of reference and deformed images, since the goal is to introduce and highlight the benefits and the important features of the technique.

E. Digital image correlation

With reference and deformed image arrays acquired, there are two options available to obtain the strain fields throughout the region of interest resulting from the applied deformation: (1) The image arrays can be stitched together to form very large images on which DIC can be performed or (2) each pair of reference and deformed images can be correlated individually, and the DIC strain fields resulting from all of the correlations can then be stitched together. For the image stitching method, a plugin for the open-source FIJI imaging software was used to stitch image arrays to form large images (with size on the order of 100 megapixels). The reference and deformed images (large stitched images) were then correlated using commercial DIC software. In the second approach, each pair of reference and deformed images (individual images, not stitched) was correlated and an in-house code was then used to stitch the results by numerically merging the data sets onto a common grid with interpolation. Both of these two stitching approaches has been demonstrated in this work and results using each method will be shown in Sec. III. An extensive discussion of the advantages and disadvantages of the two stitching procedures will be given in Sec. IV.

F. EBSD and DIC alignment

Finally, the strain and microstructure fields over the region of interest can be aligned using the fiducial markers from step 1. These fields can be related by overlaying a map of grain boundaries (from EBSD) on top of a contour plot of strain fields (from DIC). An open-source imaging program (GIMP) was used in this study to overlay EBSD and DIC images. Although markers do not appear in the strain fields themselves, the location of the strain fields is known in relation to the optical microscope reference images. To relate strain fields to microstructure, the strain fields are first overlaid onto the reference image array (the exact location of the strain field is known in relation to this image). Then the microstructural data are overlaid onto the same image array, adjusting the scale, location, and rotation of the grain boundaries map until the indentation marks are aligned. The resulting plots of grain boundaries overlaid onto strain fields, examples of which are shown in Figs. 3 and 4, can then be used

TABLE I. Measurement resolution properties at several magnifications for a camera with a pixel size of 4.4 μm.

Magnification	Field of view (μm)	Scale (μm/pixel)	Subset size at 101 pixels (μm)	Ratio of grain area to subset area
1×	7000×5200	4.4	440	0.04
5×	1400×1100	0.88	89	0.90
14×	530×400	0.31	33	7.2
31×	220×170	0.14	14	35
50×	140×100	0.087	9	92

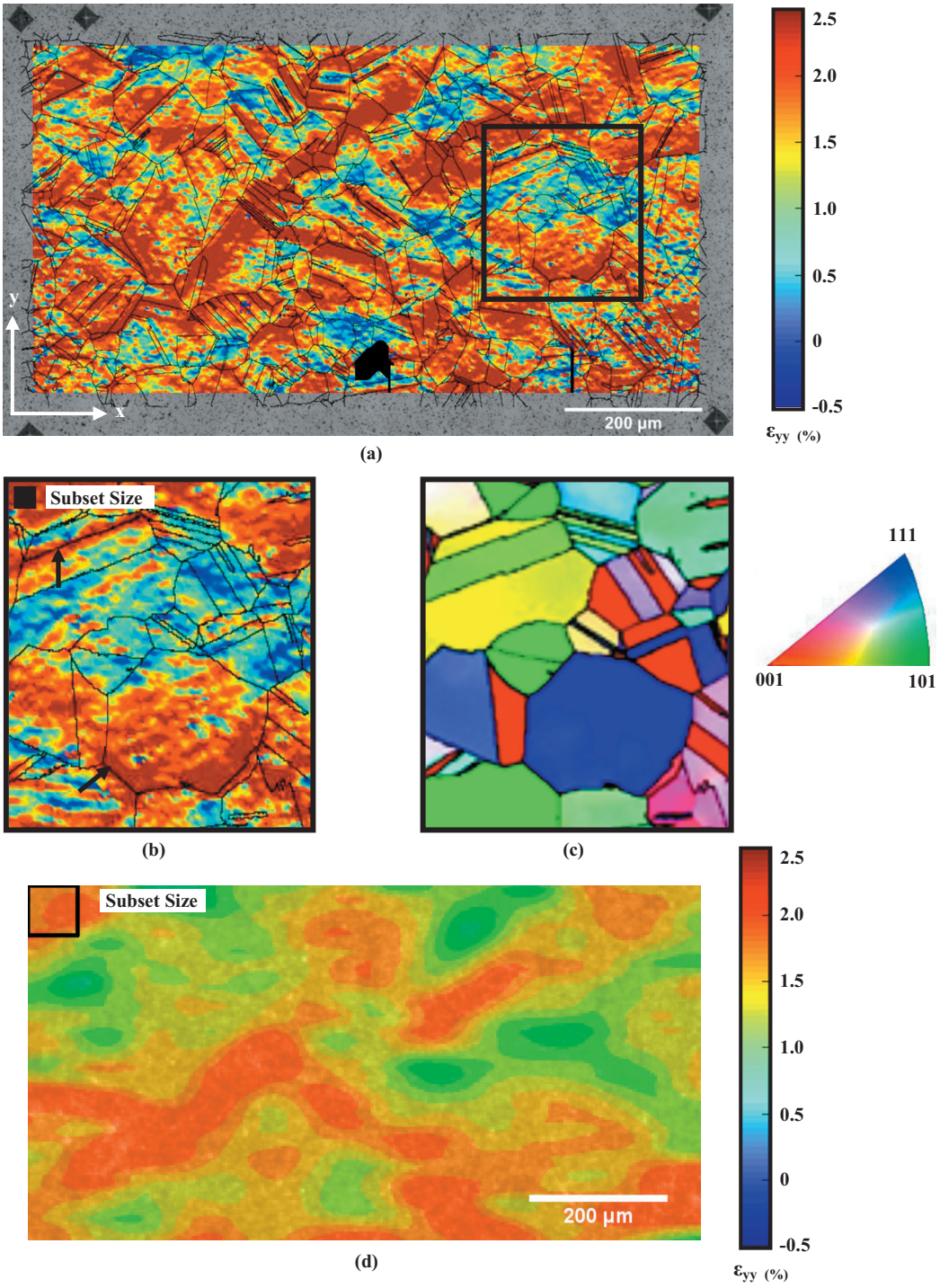

FIG. 3. (Color) (a) Contour plot of the ε_{yy} strain field with overlaid grain boundaries. The reference and deformed images are a composite of 316 images at 31× magnification (*ex situ*). (b) A portion of the contour plot in (a) is magnified to show the strain localizations that can be resolved with this technique. Note the arrows indicating localization at a twin and a grain boundary. (c) Grain orientation map of the region shown in (b). (d) Contour plot of the ε_{yy} strain field at low magnification (5×) of the same region shown in (a). Note that the subset size in (b) is much smaller than the one used in (d), which results in higher resolution fields with subgrain level accuracy.

to draw conclusions about the effects of microstructure on strain accumulation.

III. APPLICATIONS OF *EX SITU* METHOD

In this paper, two specific examples will be given to demonstrate the method's feasibility. In Sec. III A, the technique is used to capture residual strains from cyclic plasticity using the first stitching technique described in Sec. II E (i.e., stitching optical images and then correlating). The example in Sec. III B applies the technique to a fatigue crack growth experiment using the second stitching technique, i.e., stitching DIC strain fields from correlations of individual image pairs. For these two examples, polycrystalline specimens with an average grain size of roughly 100 μm and random texture orientation were used. The material in both cases was the nickel-based superalloy, Hastelloy X.

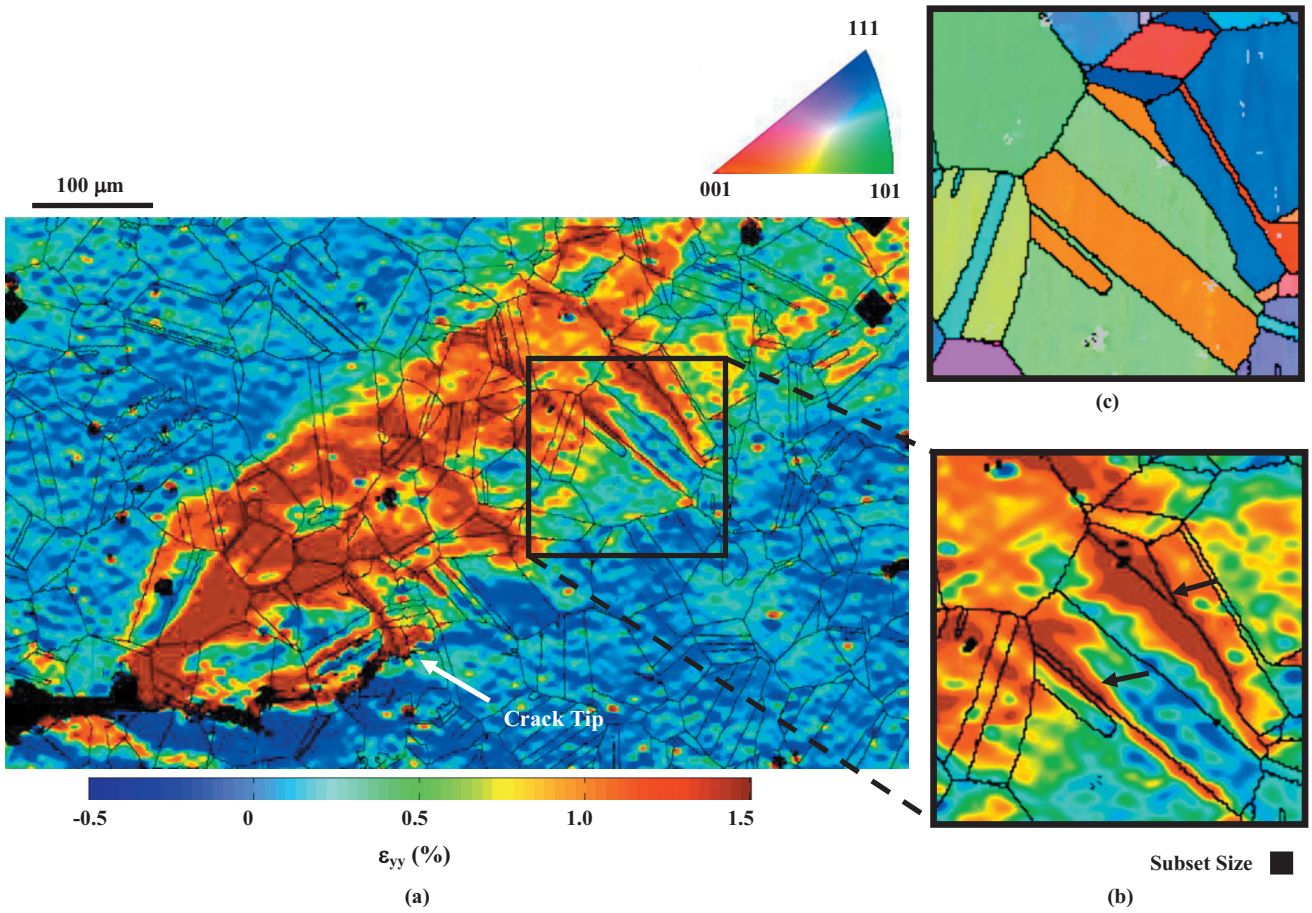

FIG. 4. (Color) Contour plot of the ε_{yy} strain field around the tip of a fatigue crack with overlaid grain boundaries (a combination of 112 DIC results at 50× magnification). Only the upper half of the field is shown here to increase the detail that can be seen (note the upper three of five indentation marks). (b) A portion of the contour plot is magnified to show the strain localizations that can be resolved with this technique. Note the strain concentrations on two grain boundaries indicated by arrows. (c) Grain orientation map of the region shown in part (b).

A. Cyclic plasticity with image stitching

Plastic strain localization in a dog bone specimen has been studied using the *ex situ* procedure described in Sec. II. The specimen was incrementally loaded in uniaxial tension to 2%, 3.8%, and 5.6% nominal plastic strains. High magnification (31×) DIC measurements were obtained *ex situ* at the end of each loading cycle, and lower magnification (5×) *in situ* measurements were obtained in real time throughout each loading cycle. Since the emphasis in this section is to show feasibility of the *ex situ* method, only results from the first loading cycle (2% strain accumulation) will be presented. A 1000×600 μm^2 region of interest at the center of the specimen gage area was observed. Reference images were taken in the optical microscope at 31× magnification (0.14 μm/pixel). A total of 316 overlapping images were captured and stitched together to cover the area of interest.

In the first loading cycle, the specimen was loaded with a strain rate of 1.83×10^{-4} s^{-1} to 2.2% nominal strain (in position control) which corresponded to a stress of 465 MPa. To ensure that the specimen does not go into compression during unloading, the specimen was unloaded in load control to a final setpoint of 0 KN. After unloading, the total residual strain was 2% nominal strain measured using a 1/2 in. gauge length extensometer. Subsequently, 316 deformed images were captured and stitched following the same procedure used for the reference images. In plane displacements and strains were calculated using a commercial DIC software (Vic2D from Correlated Solutions). Grain boundaries from EBSD were overlaid onto the ε_{yy} strain field (vertical strains along loading axis), as shown in Fig. 3(a), and aligned using the Vickers indentation marks.

Using this method, strain localizations can be detected and quantified in relation to the microstructure. For example, in the region shown in Figs. 3(b) and 3(c), strain localization on grain and twin boundaries has been precisely measured. Also the local heterogeneous material response can be observed, measured, and directly related to the microstructure. [Notice regions of high and low strains in Figs. 3(a) and 3(b).]

The advantage of this *ex situ* method is illustrated by comparing the *ex situ* (high magnification) strain field in Fig. 3(a) to the *in situ* (low magnification) strain field over the same area in Fig. 3(d). With the higher resolution *ex situ* images (at 0.14 μm/pixel), details can be captured with subgrain level accuracy that are not visible in the *in situ* results (at 0.88 μm/pixel). This enables quantitative analysis of the plastic strain fields in relation to the microstructure of the polycrystalline specimen. Different aspects of the microstructure, such as grain boundaries and grain orientation, and how they affect plastic strain accumulation, can then be in-

vestigated. Note, however, that the *in situ* results also contain elastic strain which is not visible with the *ex situ* technique.

B. Fatigue crack growth with DIC stitching

A single edge notch tension specimen of Hastelloy X was prepared as outlined in Sec. II. The specimen was fatigue loaded at a rate of 2 Hz in a servohydraulic load frame to initiate and grow a fatigue crack through the region of interest. The specimen dimensions are $50\times9\times3$ mm^3 with a notch that runs 1.5 mm through the width of the specimen. The region of interest, framed by Vickers microindentation marks, has dimensions of 700×800 μm^2 and is located 3.05–3.75 mm ahead of the notch mouth (similar to the geometry shown in Fig. 1, but with the region of interest further ahead of the notch). The specimen was loaded with a nominal stress intensity range ΔK, of 19 MPa$\sqrt{\text{m}}$, and a load ratio R (minimum to maximum load) of 0.1. For the results shown here, reference images were captured just after crack initiation and deformed images were taken roughly 223 000 cycles later at a total crack length (notch plus fatigue crack) of 3.38 mm. At this length, the crack had grown halfway through the region of interest. To cover the region of interest, image sets consisting of 112 *ex situ* images were captured at $50\times$ magnification (0.087 μm/pixel) resulting in a subset size of 9 μm and a subset spacing of 0.9 μm. DIC was performed separately on each of the 112 pairs of images and the second stitching method (Sec. II E) was used to obtain strain fields over the region. A plot of the resulting ε_{yy} strain field is shown in Fig. 4(a) with an overlay of grain boundaries obtained from 12 EBSD scans. To increase the amount of detail visible in this plot, only half of the region of interest is shown. With grain boundaries and DIC strain fields aligned, microstructural geometry can be compared to accumulated strain. An example of this is shown in Figs. 4(b) and 4(c) where two strain localizations on grain boundaries are measured. Furthermore, since EBSD provides grain orientation information [Fig. 4(c)], other factors besides grain boundary locations could also be investigated.

IV. DISCUSSION

As mentioned in Secs. II and III, data stitching can be done in two ways: stitching images before correlation or stitching DIC strain fields after correlation. Each of these methods has advantages and disadvantages. The first approach to obtaining a DIC strain field over the entire region of interest is to stitch the reference and deformed image arrays together to form large images on which DIC is performed (see Fig. 3 for results using this approach). The main benefit of this method is that it requires less human intervention. After the automated stitching process, only one DIC correlation needs to be performed. A drawback of this method is that in can only be used at relatively high levels of nominal strain (above 1%). This limitation arises from the noise introduced by imperfect image stitching. Such noise is demonstrated in the contour plots of Fig. 5, in which four reference and four deformed images, with no loading between images, are stitched into image arrays and correlated. The stitching software uses a Fourier-based stitching algorithm that theoretically locates images with respect one another with subpixel accuracy. However, the real stitching error is enough to be detected by DIC since it possess subpixel accuracy. Since the reference and deformed image arrays are stitched independently of one another, the stitching error will be different for each image array (i.e., an individual image in the reference array may be placed at a location that is a fraction of a pixel different from its corresponding image in the deformed array). While a stitching error of a fraction of a pixel is a small error for image appearance, it is a large error in DIC displacements as seen in the stitched image DIC results of Fig. 5.

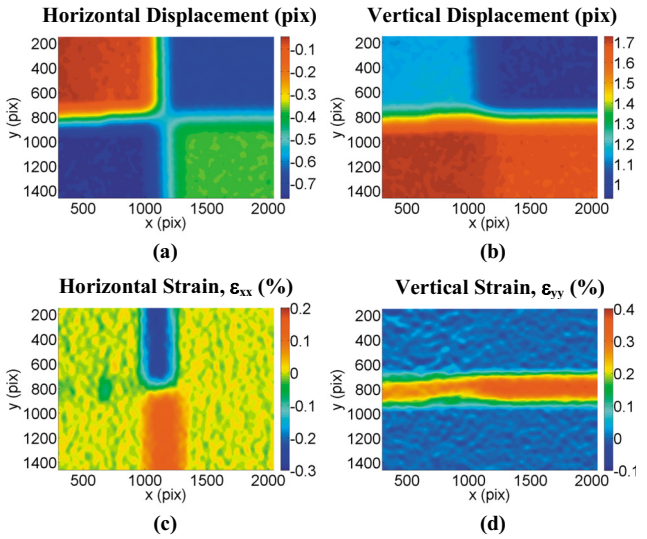

FIG. 5. (Color online) DIC strain artifacts due to stitching error for a set of four images. No loading took place between the reference and deformed images. The specimen was simply removed and reinserted into the microscope. Strain artifacts [Figs. 3(c) and 3(d)] appear because the relative displacement between each corresponding reference and deformed image in the set is different [Figs. 3(a) and 3(b)].

The DIC displacement fields in Figs. 5(a) and 5(b) show that displacements, i.e., image location error, for each of the four images are each slightly different by fractions of a pixel. When the strain is computed from these DIC displacement fields, the subpixel locating errors lead to bands of strain with a magnitude near 0.2% on the image seams, which is significantly larger than the 0.05% background noise. These strain bands arise because strain is calculated by differentiating the displacement field and is therefore very sensitive to the displacement gradient caused by image stitching error. Since the horizontal strain ε_{xx} is computed by differentiating the displacement field horizontally, error only occurs when this differentiation moves horizontally across an image seam; hence, only the vertical image seams are apparent in the plot of ε_{xx}. Similarly, only horizontal seams are apparent in the plot of ε_{yy} strain.

The error introduced by stitching can be safely neglected at increased levels of average nominal strain (the example shown in Fig. 5 is at 0% nominal strain). The strain fields in Fig. 6 were created by incrementally loading a specimen and applying the *ex situ* procedure with the first method of image stitching. As shown in Figs. 6(a)–6(d), which correspond to an average residual strain of 0.23%, 0.36%, 1.08%, and

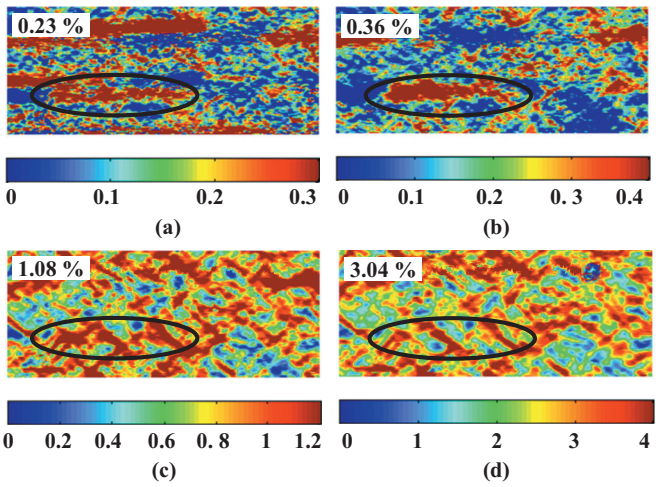

FIG. 6. (Color) Contour plots of ε_{yy} strain fields at various global strain levels created by stitching 15 images together before correlating. Strain fields with global strains of (a) 0.23%, (b) 0.36%, (c) 1.08%, and (d) 3.04%. As global strain increases, strain artifacts due to stitching become less dominant. Stitching strains become negligible around 1% global strain.

3.04%, respectively, strains arising from stitching errors are the dominant feature at low global strain levels, but become almost undetectable as the global strain increases. These artifacts diminish as the signal to (stitching) noise ratio becomes larger. By 1% average strain, the stitching error is barely visible, and by 3% average strain, it has essentially disappeared entirely. This indicates that stitching images before performing DIC will work adequately when the strain throughout the region of interest is relatively large (more than 1% or so). However, if the global strain is less than 1% or if the strain field contains large regions of low strain, then the effects of image stitching must be considered.

A proposed approach to minimize the error associated with stitching at low strain levels is by adjusting imaging parameters. To this end, experiments were performed to investigate parameters including image overlap amount and image blending algorithm. In Fig. 6, a linear blending algorithm was used in the stitching process. This algorithm computes values in the overlap region between two images by a weighted function of the proximity to the border of each image. While linear blending creates a stitched image with less visible seams, it distributes error over the entire overlap area. Thus, it appears that reducing the amount of overlap would reduce the area covered by stitching strain artifacts. Ideally, a one pixel overlap region would concentrate the entire stitching error into a small region (approximately equal to the subset size), leaving the majority of the results unaffected by stitching strains. One difficulty with this one pixel overlap approach results from the fact that there are actually two stitches performed, the reference and deformed images, meaning that there are actually two seams causing strain artifacts. This fact is not apparent when the overlap is large and the seams are wide, but if the overlap is small and the reference and deformed seams are not at the same exact locations, then two sets of strain bands will appear: one at the deformed image seams and one at the reference image seams.

If stitching artifacts could actually be limited to small portions of the correlation region with the methods described above, it is possible that these artifacts, with their locations known, could be accounted for. A simple approach to obtain a trustworthy strain field would be to simply delete the data at the stitching locations giving a strain field with lines of missing data. A more thorough approach would be to replace the strain data in the stitching regions with reliable DIC strains. This could be accomplished by having two sets of reference and two sets of deformed images offset by half an image in each direction. By combining the DIC results from each of these arrays, reliable DIC strains could be determined throughout the entire correlation region without any missing data. This process would be time consuming since it requires locating each image seam and performing two sets of image correlations for each set of data. It was therefore not pursued here in favor of the alternative approach of the second stitching methodology, which will now be discussed.

The second approach to obtaining a single strain field over the region of interest is to correlate each individual deformed image separately with its corresponding reference image and then stitch the DIC results together. This approach is more time consuming because it requires the user to perform hundreds of DIC correlations instead of just one, but as will be seen, it provides results that are more trustworthy than the image stitching method. Each deformed image was inevitably captured at a slightly different location from its reference image, thus each correlation gives a different rigid translation in the DIC displacement field results. Stitching these displacement fields together is problematic because, as in the first image stitching method, very sharp gradients will occur at the seams. However, since strain is unaffected by rigid motion, strain fields do not have discontinuities at image boundaries. Stitching *strains* takes place after DIC is performed; consequently, there is no chance for the stitching procedure to affect the magnitude of the strain field. The only possible error caused by stitching in this manner is in the location of each strain field. The relative location of each strain field must be known in order to stitch them into a larger field. These locations can be easily obtained by stitching the reference images together to form the reference image array used in stitching approach 1. The image stitching program locates images with respect to one another with subpixel accuracy and the locations of the DIC strain fields within these reference images are known exactly so the position of each strain field with respect to one another is known with subpixel accuracy. The relative locations of strain fields are rarely multiples of the subset spacing so strain fields are interpolated to an evenly spaced grid, which makes data processing more efficient. Although strain fields are interpolated, the interpolation error generated is not nearly as large as the interpolation error of stitching images before correlation. Evidence of this is the plot in Fig. 4(a) which is a product of DIC strain field stitching. The fact that seams are not visible in this image, even in areas of low strain, shows that adjacent correlations were in agreement and stitched successfully. One minor drawback of this approach is that it requires more image overlap (possibly requiring more images to be captured for the same region). This is because of the fact that the DIC regions of each

image, which are always smaller than the images themselves, must overlap. Despite the extra work involved with this approach, it is relatively simple and it provides a trustworthy strain field, free of stitching artifacts, which can be compared to full-field microstructural measurements (Fig. 4). Its drawback, however, is the inability to provide displacement measurements.

V. CONCLUSIONS

An *ex situ* method was developed for linking DIC strain measurements to microstructure geometry and orientation from EBSD results. Vickers indentation marks were found to work well for aligning these two fields. High spatial resolution strain measurements were made over relatively large regions using data stitching. Stitching images together *before* performing DIC resulted in artificial bands of high and low strain due to stitching inaccuracies. When the average strain in the region is larger than roughly 1%, these artifacts become negligible compared to the actual strain field. For strain fields with an average strain of less than 1%, artifacts can be eliminated by stitching DIC strain fields after correlation. Two applications of this *ex situ* technique were shown, one using each of these data stitching techniques. In the first investigation, cyclic plasticity was observed on a specimen with relatively large average strains using image stitching. High resolution strain measurements were compared to grain boundaries over a region of roughly $500 \times 960\ \mu m^2$ (Fig. 3). These high magnification *ex situ* results were shown to have much better spatial resolution than *in situ* results over the same region [Figs. 3(a) and 3(c)]. In the second investigation, strain fields near a fatigue crack tip were observed and overlaid with grain boundaries. DIC strain field stitching was required since large portions of the strain field were less than 1%. Enlarging a region of the results showed that strain localizations along grain and/or twin boundaries can be detected with this technique [Fig. 4(b)]. As these two investigations showed, this *ex situ* technique provides pointwise comparisons between strain fields and microstructure that will enhance understanding of materials behavior at the microstructural level. Clearly, this process is valid for surface measurements. Internal measurements combining DIC and EBSD are more cumbersome since they would require sample sectioning, but are also possible.[27]

ACKNOWLEDGMENTS

This work was supported by the Midwest Structural Sciences Center (MSSC), which is supported by the Air Vehicles Directorate of the U.S. Air Force Research Laboratory under Contract No. FA8650-06-2-3620. The guidance and support of Dr. Ravi Chona and Dr. Stephen (Mike) Spottswood at the Air Force Research Laboratory is greatly appreciated. Assistance with loading hardware and software was provided by Rick Rottet and Dr. Peter Kurath. EBSD results were obtained with the assistance of Jim Mabon at the Frederick Seitz Materials Research Laboratory Central Facilities, University of Illinois, which are partially supported by the U.S. Department of Energy under Grant Nos. DE-FG02-07ER46453 and DE-FG02-07ER46471.

[1] G. Sachs, VDI Z. (1857-1968) **72**, 734 (1928).
[2] G. I. Taylor, J. Inst. Met. **62**, 307 (1938).
[3] J. F. W. Bishop and R. Hill, Philos. Mag. **42**, 414 (1951).
[4] P. Van Houtte, A. K. Kanjarla, A. Van Bael, M. Seefeldt, and L. Delannay, Eur. J. Mech. A/Solids **25**, 634 (2006).
[5] A. Molinari, G. R. Canova, and S. Ahzi, Acta Metall. **35**, 2983 (1987).
[6] A. J. Beaudoin, P. R. Dawson, K. K. Mathur, and U. F. Kocks, Int. J. Plast. **11**, 501 (1995).
[7] C. A. Bronkhorst, S. R. Kalidindi, and L. Anand, Philos. Trans. R. Soc. London, Ser. A **341**, 443 (1992).
[8] J. D. Clayton, B. M. Schroeter, D. L. McDowell, and S. Graham, ASME J. Eng. Mater. Technol. **124**, 302 (2002).
[9] F. Barbe, S. Forest, and G. Cailletaud, Int. J. Plast. **17**, 537 (2001).
[10] Z. Zhao, M. Ramesh, D. Raabe, A. M. Cuitino, and R. Radovitzky, Int. J. Plast. **24**, 2278 (2008).
[11] T. Merzouki, C. Collard, N. Bourgeois, T. B. Zineb, and F. Meraghni, Mech. Mater. **42**, 72 (2010).
[12] E. Héripré, M. Dexet, J. Crépin, L. Gélébart, A. Roos, M. Bornert, and D. Caldemaison, Int. J. Plast. **23**, 1512 (2007).
[13] F. Delaire, J. L. Raphanel, and C. Rey, Acta Mater. **48**, 1075 (2000).
[14] A. E. Bartali, V. Aubin, and S. Degallaix, Int. J. Fatigue **31**, 2049 (2009).
[15] M. A. Tschopp, B. B. Bartha, W. J. Porter, P. T. Murray, and S. B. Fairchild, Metall. Mater. Trans. A **40**, 2363 (2009).
[16] W. Tong, Exp. Mech. **37**, 452 (1997).
[17] C. Efstathiou, H. Sehitoglu, and J. Lambros, Int. J. Plast. **26**, 93 (2010).
[18] H. Padilla, J. Lambros, A. Beaudoin, and I. M. Robertson, Int. J. Solids Struct. "Use of multiscale image correlation to study the relationship between inhomogeneous deformation and local texture in zirconium" (submitted).
[19] D. Raabe, M. Sachtleber, Z. Zhao, F. Roters, and S. Zaefferer, Acta Mater. **49**, 3433 (2001).
[20] M. A. Sutton, W. J. Wolters, W. H. Peters, and W. F. Ranson, Image Vis. Comput. **1**, 133 (1983).
[21] M. Sachtleber, Z. Zhao, and D. Raabe, Mater. Sci. Eng., A **336**, 81 (2002).
[22] N. Zhang, Int. J. Plast. **20**, 523 (2004).
[23] A. Tatschl and O. Kolednik, Mater. Sci. Eng., A **339**, 265 (2003).
[24] J. Abanto-Bueno and J. Lambros, Exp. Mech. **45**, 144 (2005).
[25] V. Randle and O. Engler, *Introduction to Texture Analysis* (CRC Press, Boca Raton, 2000).
[26] K. N. Jonnalagadda, I. Chasiotis, S. Yagnamurthy, J. Lambros, J. Pulskamp, R. Polcawich, and M. Dubey, Exp. Mech. **50**, 25 (2010).
[27] D. P. Field, K. R. Magid, I. N. Mastorakos, J. N. Florando, D. H. Lassila, and J. W. Morris, Jr., Philos. Mag. **90**, 1451 (2010).